

A Piezoresistive Cantilever Force Sensor for Direct AFM Force Calibration

Jon R. Pratt¹, John A. Kramar¹, Gordon A. Shaw¹, Douglas T. Smith¹, and John M. Moreland²

¹National Institute of Standards and Technology, Gaithersburg, MD, 20899

²National Institute of Standards and Technology, Boulder, CO, 80305

ABSTRACT

We describe the design, fabrication, and calibration testing of a new piezoresistive cantilever force sensor suitable for the force calibration of atomic force microscopes in a range between tens of nanonewtons to hundreds of micronewtons. The sensor is calibrated using the NIST Electrostatic Force Balance (EFB) and functions either as a force reference or stiffness artifact that is traceable to the International System of Units. The cantilever has evenly spaced fiducial marks along its length. We report stiffnesses that vary quadratically with location, from a high of 12.1 N/m at the first fiducial to a low of 0.394 N/m at the last; with force sensitivities that vary linearly, ranging from 18.1 Ω /mN to 106 Ω /mN. We also test the device to transfer the unit of force to an atomic force microscope, finding that force and stiffness based approaches yield independent estimates of the contact force consistent within 2 % of each other.

INTRODUCTION

The desire among researchers and industry to measure forces that are traceable to the International System of Units (SI) using an atomic force microscope (AFM) has prompted national metrology institutes to explore new metrologies, including sub-micronewton force realizations [1,2], a quantum-based piconewton [3], a microelectromechanical nano-balance [4], and a variety of reference cantilevers with techniques and apparatuses for calibrating their stiffnesses and/or force sensitivities [5-9]. NIST has shown that one method for obtaining a traceable force calibration is to simply press the AFM probe against a calibrated piezoresistive cantilever force sensor [9]. This approach bypasses the problems associated with calibrating the optical lever as a displacement sensor [10]. Previously, we were constrained by the size and mechanical stiffness of the piezoresistive cantilevers that were commercially available. Here, we seek to address this limitation, and present the design, calibration, and performance testing of a new piezoresistive cantilever force transducer, or PFT, fabricated at NIST.

DESIGN AND FABRICATION OF THE PIEZORESISTIVE FORCE TRANSDUCER

Piezoresistive cantilever force sensors for AFM were first demonstrated by Tortonese, *et al.* [11] and a low frequency force sensitivity of 8 fN was achieved by Harley and Kenny [12]. Typically, two legs support a beam, with the sensors on the surface of the legs. If the legs are thinner than the beam, they form a hinge where the bending occurs, increasing sensitivity [13]. The NIST PFT shown in Figure 1 employs this last approach, and is akin to devices proposed by the Physikalisch Technische Bundesanstalt (PTB) in Germany [6], and by the National Physical Laboratory in the UK [8] for AFM force and stiffness calibration, respectively.

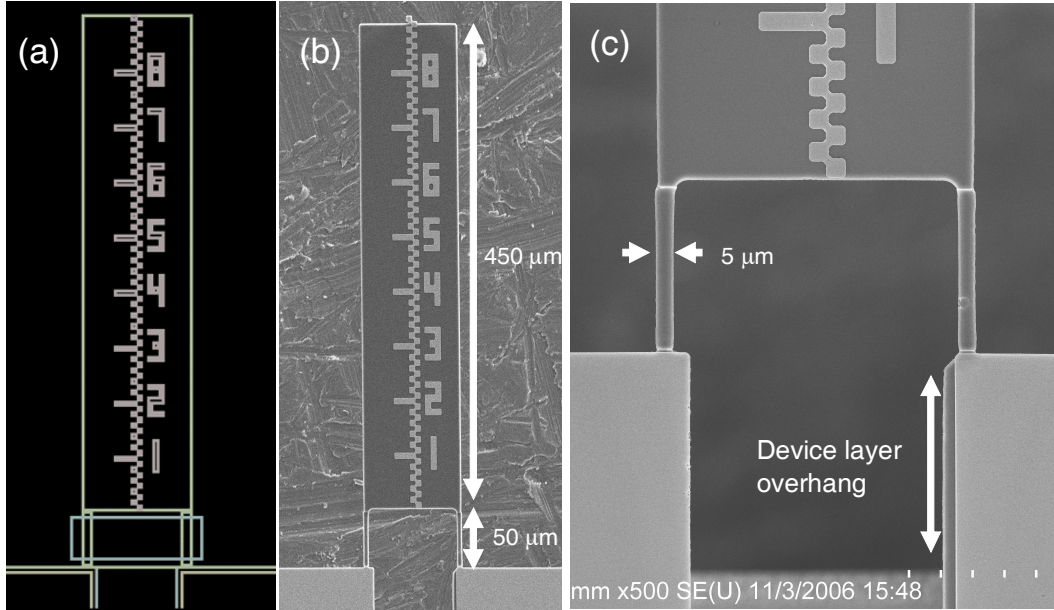


Figure 1. NIST Piezoresistive Force Transducer (PFT) (a) Mask for lithography (b) SEM image of device (c) magnified image of legs showing device layer overhang.

PFT design and fabrication

The working formula for a two leg piezoresistive sensor of the type shown in Figure 1 is

$$\frac{\Delta R}{R} = \frac{6\beta\pi_L l}{wt^2} \Delta F$$

where w , l , and t are the leg width, length, and thickness, respectively, π_L is the piezoresistive sensor coefficient, β is an ideality factor ranging from 0 to 1 depending on doping profile through the sensor, and ΔF is a force applied at the end of the legs where they support the beam [12]. In the limit that the piezoresistive sensor layer is much thinner than the leg thickness t , then $\beta = 1$. Given the parameters of $l = 50 \mu\text{m}$, $w = 5 \mu\text{m}$, $t = 3 \mu\text{m}$, $\beta = 1$, $\pi_L = 4.5 \times 10^{-10} \text{ m}^2/\text{N}$ (for $10^{19}/\text{cm}^3$ doping levels) and $\Delta F = 1 \text{ nN}$, then theoretically $\Delta R/R = 3 \times 10^{-5}$, which is detectable using a high quality ohm meter and four-terminal resistance measurement.

A preliminary fabrication process has been developed based on a silicon on insulator (SOI) wafer with a $\langle 100 \rangle$ Si device layer ($6 \mu\text{m}$) with a resistivity of $> 10\,000 \Omega\cdot\text{cm}$ bonded to a $3 \mu\text{m}$ oxide layer on a $\langle 100 \rangle$ Si handle wafer ($400 \mu\text{m}$) with a resistivity of $10 \Omega\cdot\text{cm}$. The basic concept is to pattern the cantilevers in the device layer, release them using a deep reactive ion etch (DRIE) followed by a wet buffered HF oxide etch to remove the oxide, and a final acetone soak to release individual devices from the DRIE mounting wax. The essential elements of the fabrication process are shown in Figure 2.

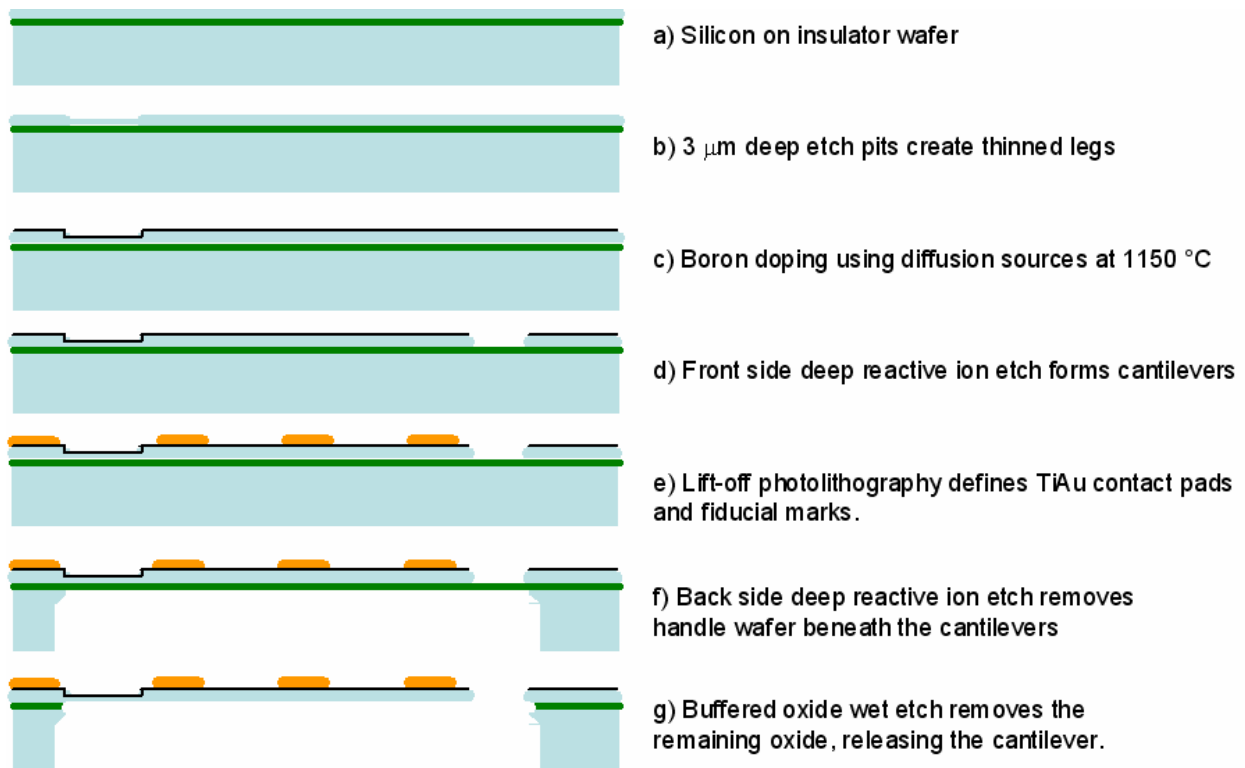


Figure 2. PFT fabrication process.

PFT CALIBRATION AND RESULTS

The PFT's force sensitivity s_P and stiffness k_P were calibrated at each fiducial by pressing against the NIST EFB [1,2,8]. An etched platinum tip was mounted as an indenter on the EFB and used to probe the PFT at the titanium gold fiducial marks. We noted that the tip tended to adhere to the gold, and more consistent results were obtained by pressing on the "silicon," laterally away but even with the gold fiducials. Cross-axis sensitivities of the PFT to off-axis loading (e.g., combined torsion and bending) were investigated, but are not reported here. The test locations proved easy to find in subsequent AFM scans, since the EFB probe tip marred the PFT surface wherever the two came into contact. Thus, it was possible for the AFM to find and probe the actual calibration locations on the silicon, rather than at the lithographically defined fiducials, during the performance test (see next section).

To begin a calibration, the EFB tip was brought up to the PFT under interferometer position control until contact was detected, for example by a change in the piezoresistance, and then the position adjusted to an initial PFT deflection of typically 0.1 μm . The EFB was then cycled into the PFT over a stroke of between 0.8 μm (at Fiducial 1) and 4 μm (at Fiducial 8) at a rate of one cycle every five to ten minutes, for varying numbers of cycles ranging from four to 140. EFB force and displacement, and the PFT resistance were recorded at prescribed displacements during each cycle. On pull-off, an attractive force of order 0.1 μN was typically detected as a negative deflection of the PFT. Long-term force and resistance background drift are subtracted from the data, and the data are averaged. As discussed in [1], it is necessary to characterize the stiffness of the EFB, and to subtract the force needed to deflect it, when using the EFB as an instrumented indentation machine. The EFB stiffness, k_{EFB} , was measured to be (7 ± 2) mN/m for a 4 μm stroke, which is at most a 2 % correction for the weakest k_P measured at Fiducial 8.

Data acquired at Fiducial 5 are typical, and are shown in Figure 3. The stiffness and sensitivity at all eight fiducials are listed in Table 1. The listed uncertainties are the statistical variations from averaging the cycles. The uncertainties in the forces and distances generated by the EFB are at least an order of magnitude less. The dependence of the sensitivity on the location along the PFT was examined and found essentially linear, with slope of $12.53 \text{ } \Omega/\text{mN}/U$, where U is the fiducial unit distance, nominally $50 \text{ } \mu\text{m}$. Residuals from a linear fit to the sensitivity are also listed in Table 1. Most are within the statistical component of the uncertainty. If the PFT is modeled as a hinge with torsional stiffness κ supporting a rigid lever, the balance of moments for small displacements leads to the equation $k_p(L) = \kappa / L^2$, where $k_p(L)$ is the effective stiffness of pressing into the cantilever at a distance L from the effective hinge location. This predicted $1/L^2$ dependence of the stiffness is also well matched by the data. The trends in the residuals listed in Table 1 are an indication of the limitations of the simplifying assumptions in the models.

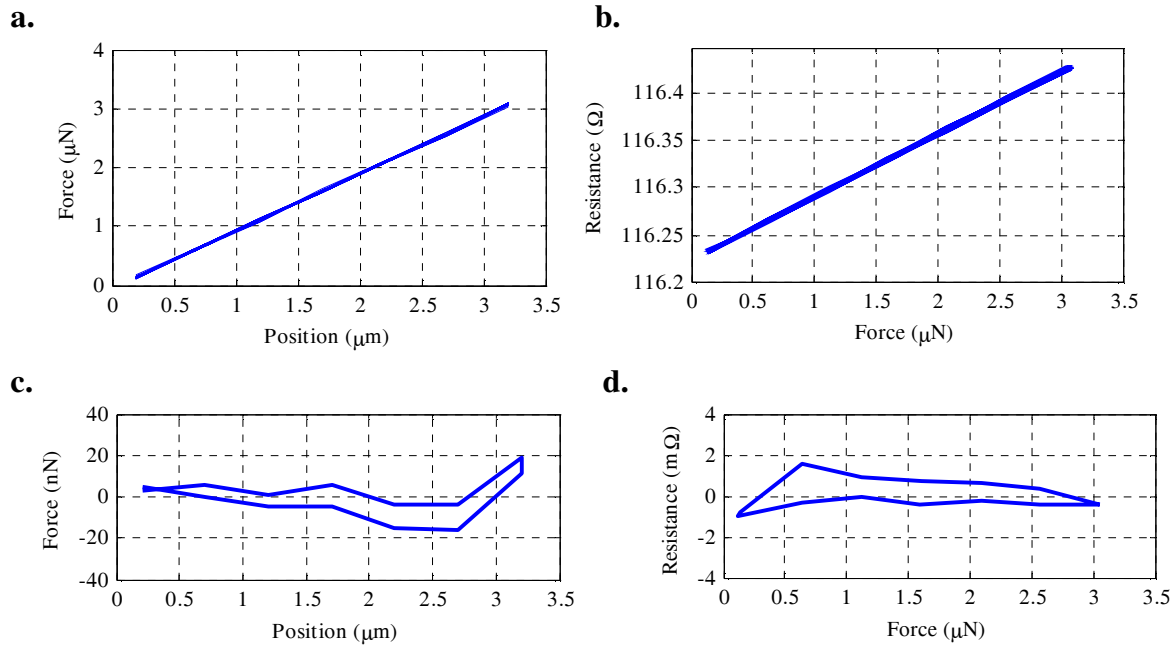


Figure 3. The PFT response at Fiducial 5: **a.** force as a function of displacement (19 cycles) **b.** resistance as a function of force, and **c.** and **d.** cycle-averaged residuals after linear fits.

Table 1. Stiffness and sensitivity of the PFT as measured using the EFB.

Fiducial	Stiffness (N/m)	$(1/L^2)$ Fit (N/m)	Residual (N/m)	Sensitivity (Ω/mN)	Linear Fit (Ω/mN)	Residual (Ω/mN)
1	12.1 ± 0.2	12.9	-0.78	18.1 ± 0.2	17.8	0.26
2	4.60 ± 0.02	4.62	-0.021	30.4 ± 0.2	30.3	0.10
3	2.382 ± 0.006	2.357	0.025	42.8 ± 0.3	42.9	-0.06
4	1.437 ± 0.003	1.425	0.013	55.5 ± 0.3	55.4	0.14
5	0.966 ± 0.004	0.953	0.013	67.6 ± 0.6	67.9	-0.38
6	0.692 ± 0.004	0.682	0.0092	79.3 ± 0.6	80.5	-1.17
7	0.510 ± 0.002	0.512	-0.0029	93.8 ± 0.8	93.0	0.78
8	0.394 ± 0.001	0.399	-0.0049	105.8 ± 0.7	105.5	0.33

AFM CONTACT FORCE CALIBRATION AND RESULTS

The PFT was used to calibrate contact forces produced by an AFM. Two procedures were investigated, one employing the PFT as a force reference, the other as a stiffness reference. For both procedures, the tip of the AFM's cantilever was positioned into contact with the PFT using the microscope coarse and fine motion stages. Fiducial marks 2, 4, and 8 were chosen as trial locations for the purposes of performance testing. A topographic AFM image was obtained near the fiducial marks to precisely locate the point at which the PFT had been calibrated, allowing the tip of the AFM cantilever to be positioned within approximately 100 nm of the point calibrated by the EFB.

Once positioned over a calibration point, the AFM cantilever was raised until it was just out of contact with the PFT surface. This out of contact position was used to subtract the effects of thermal drift in the PFT and optical lever signals. A linear variable differential transformer (LVDT) sensor integrated with the AFM z -scan axis allowed the precise maintenance of this reference during the experiments. Next, the AFM probe tip was brought into contact with the PFT surface, and a series of five increasing loads was applied with a return to the out of contact position between each load. The loads were feedback-controlled based on the optical lever signal. At each load, and at the reference steps between them, the optical lever signal, the AFM z position, and the resistance of the PFT were each consecutively averaged over approximately five seconds. The resistance of the reference cantilever was determined with a four-terminal measurement. The optical lever signal and AFM z position data were collected using the AFM controller electronics. The optical lever signal was the measured signal from the AFM four-quadrant photodetector, and the z position was the measured signal from the AFM z -axis LVDT sensor. Five seconds were allowed after each change in load to let the piezoresistor equilibrate. This experiment was repeated ten times at each trial location. The effects of thermal drift were minimized by subtracting the measurements performed at the neighboring reference positions from those performed at a given load, as is shown in Figure 4. The changes in PFT resistance ΔR_P , optical lever signal ΔV_{OL} , and z -axis position Δz , were then determined relative to the lowest applied load at each location, i.e., load 1 in Figure 4.

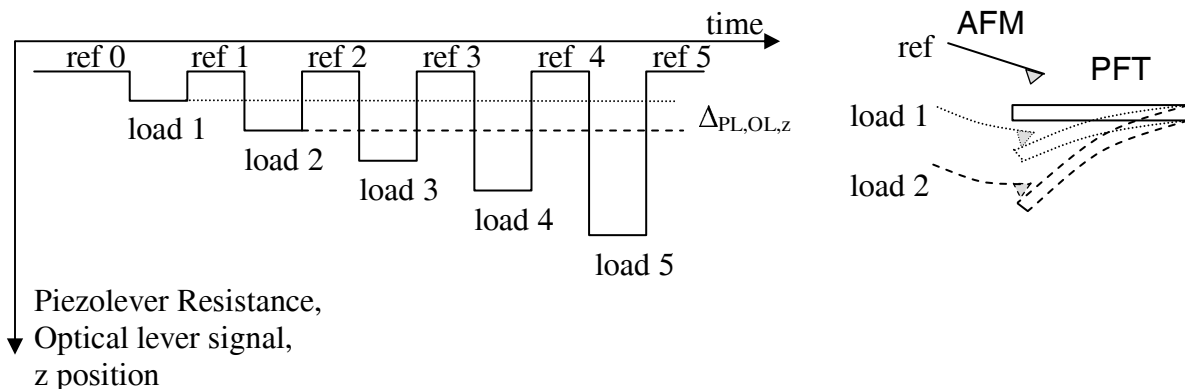


Figure 4. Calibration of AFM optical lever detector with the PFT. A series of increasing loads (1 to 5) are applied to the PFT by the AFM. Piezoresistance, optical lever signal, and z position of the AFM are recorded.

The conversion of ΔR_P into change in contact force F_R was carried out using the appropriate sensitivity value s_P determined with the EFB such that

$$F_R = \Delta R_P s_P$$

A separate estimate of the contact force, F_k , was determined using the spring constant of the PFT, k_P , as measured previously by the EFB, and the AFM cantilever deflection as measured by the optical lever detector. If a rigid contact between the AFM and reference cantilever is assumed, the change in contact force between different loading steps can be calculated using

$$F_k = k_P (\Delta z - \Delta V_{OL} s_{OL})$$

where Δz is the change in AFM z -axis position between loads as measured by the AFM's internal LVDT position sensor, and s_{OL} is the sensitivity of the optical lever signal to displacement. This sensitivity was determined by pressing against the rigid base of the PFT using the same loading sequence described in Figure 4.

The results of the contact force measurement are shown in Figure 5. The force calibration of the optical lever arm detector voltage signal (OL signal) for the two methods are compared at each fiducial mark tested. Error bars are shown for each method and indicate the statistical component of the standard uncertainty with a coverage factor of one. The slope of the plots in Figure 5 yields the force sensitivity of the AFM optical lever. Averaging the three values obtained at each fiducial yields $0.164 \mu\text{N/V} \pm 0.005 \mu\text{N/V}$ and $0.167 \mu\text{N/V} \pm 0.004 \mu\text{N/V}$ for the calibration using F_k and F_R , respectively. The uncertainties reported are the standard deviations of the values measured at the three fiducials tested.

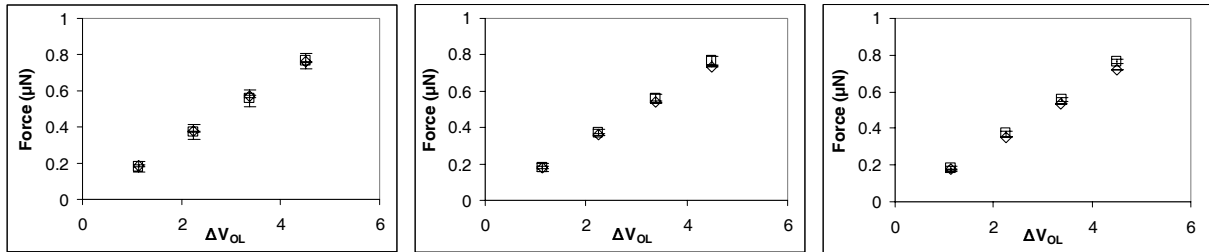


Figure 5. Force calibration of an AFM optical lever signal. Figures from left to right show the calibration results using fiducial marks 2, 4 and 8, respectively. Results are shown for the methods using the PFT as a piezoresistor (\square) and as a reference spring (\diamond).

CONCLUSIONS

We found that the measured sensitivity of the piezoresistor was a factor of 45 lower than expected. Causes are speculative, but the sensor coefficient π_L is known to vary by as much as a factor of four for doping levels ranging from 10^{19} to 10^{21} [14], the β factor can be substantially smaller if the doping profile is deeper than estimated, and the stress may have been less than expected, since the legs are attached to an overhanging section of the device layer at the base of the cantilever (see Fig. 1c). Still, the PFT calibration results are comparable to our previous experience using a commercial sensor [9], and have a much wider dynamic range, since one device now encompasses a range of sensitivities and stiffness values. Here, the most precise

sensitivity measured at Fiducial 4 had a relative standard deviation of 0.54 %, with none of the other locations exceeding 1%. The PFT also allowed the optical lever signal of an AFM to be calibrated as a force read-out device via two independent approaches, both with much better linearity and resolution than in reference [9]. The first approach, based on changes in the PFT resistance in response to probing, yields a directly traceable value of the contact forces, provided a traceable resistance measurement is available. The second approach, based on the stiffness of the PFT, can also provide a traceable value of the contact forces; however, it requires that the AFM have on-board displacement metrology, such as the LVDT on our scope. Both methods yield AFM optical lever force sensitivities that are within 1.5% of each other. Furthermore, we have shown that both the force sensitivity and stiffness of the PFT can be accurately interpolated using simple relations based on the fiducial grid that is patterned on the sensor.

ACKNOWLEDGMENTS

This work was supported by the Advanced Technology Program of NIST. The authors thank Dr. Andras Vladar for providing the SEM images.

REFERENCES

1. Pratt, J.R, Newell, D.B., Kramar, J.A., and Smith, D.T., *Meas. Sci. Technol.*, **16**, 2129 (2005).
2. Newell, D.B., Kramar, J.A., Pratt, J.R., Smith, D.T., and Williams, E.R., *IEEE Transactions on Instrumentation and Measurement*, **52**(2), 508 (2003).
3. Choi, J-H, Kim, M-S, Park, Y-K, and Choi, M-S, *App. Phys. Lett.*, **90**, 073117 (2007).
4. Cumpson, P. J. and Hedley, J., *Nanotechnology*, **14**, 1279 (2003).
5. R.S. Gates and J.R. Pratt, *Meas. Sci. Technol.*, **17**, 2852 (2006).
6. Behrens, Doering, and Peiner, *J. Micromech. Microeng.*, **13**, S171 (2003).
7. Kim, M-S, Choi, J-H, Park, Y-K, and Kim, J-H, *Metrologia*, **43**, 389 (2006).
8. Cumpson, P. J., Clifford, C. A., and Hedley, J., *Meas. Sci. and Tech.*, **15**, 1337 (2004).
9. Pratt, J.R., Smith, D.T., Newell, D.B., Kramar, J.A., and E. Whintenton, *J. Mat. Res.*, **19**(1), 366 (2004).
10. E.C.C.M. Silva and K.C.Van Vliet, *Nanotechnology*, **17**, 5525 (2006).
11. M. Tortonese, H. Yamada, R. C. Barrett, and C. F. Quate, in The Proceedings of Transducers '91 IEEE, Piscataway, NJ, 448 (1991).
12. J. A. Harley and T. W. Kenny, *App. Phy. Lett.*, **75**, 289 (1999).
13. R. Bashir, A. Gupta, G. W. Neudeck, M. McElfresh, R.Gomez, *J. Micromech. Microeng.* **10** 483 (2000).
14. O. N. Tufte and E.L Stelzer, *J. Appl. Phys.*, **34**, 313 (1963).